Molecular Crystals and Liquid Crystals Science and Technology. Section A. Molecular Crystals and Liquid Crystals

Publication details, including instructions for authors and subscription information:
http://www.tandfonline.com/loi/gmcl19

Frequency Dependent Threshold in Bend Geometry of 5CB

Shila Garg [a], Salman Saeed [a], Steven Wild [a], Erica Bramley [a] & U. D. Kini [b]

[a] Department of Physics, College of Wooster, Wooster, Ohio, 44691

[b] Raman Research Institute, Bangalore, 560 080, INDIA

Version of record first published: 04 Oct 2006

To cite this article: Shila Garg, Salman Saeed, Steven Wild, Erica Bramley & U. D. Kini (1997): Frequency Dependent Threshold in Bend Geometry of 5CB, Molecular Crystals and Liquid Crystals Science and Technology. Section A. Molecular Crystals and Liquid Crystals, 302:1, 379-384

To link to this article: http://dx.doi.org/10.1080/10587259708041851

Mol. Cryst. Liq. Cryst., 1997, Vol. 302, pp. 379–384
Reprints available directly from the publisher
Photocopying permitted by license only

FREQUENCY DEPENDENT THRESHOLD IN BEND GEOMETRY OF 5CB

SHILA GARG, SALMAN SAEED, STEVEN WILD AND ERICA BRAMLEY
Department of Physics, College of Wooster, Wooster Ohio 44691
U.D. KINI
Raman Research Institute, Bangalore 560 080, INDIA

Abstract We report the effect of electric frequency on deformation threshold in the bend Freedericksz geometry in the presence of a stabilizing magnetic field applied normal to the plates with the destabilizing electric field impressed parallel to the sample. In general, the observed threshold and deformation above it are strongly dependent on frequency and magnetic strength associated with a pretransitional field-induced biaxiality. The periodic deformation observed under a strong magnetic field has wavevector along the electric field at low frequencies. Above a cut-off frequency, the direction of the wavevector becomes normal to the electric field. Hysterisis is present between increase and decrease of voltage. At dc or low frequency excitation, there is clear evidence of hydrodynamic flow which can become turbulent for some values of parameters.

INTRODUCTION

Application of external electric (**E**) and magnetic (**B**) fields along suitable directions on nematic liquid crystals leads to a number of interesting effects many of which are well accounted for in terms of the continuum theory [1, 2]. The theoretical interpretation of static deformations under the action of **E** are involved due to the presence of flexoelectricity [3] and because of the importance of the modification of **E** inside the nematic sample caused by director gradients [4,5]. One of the commonly studied configurations for 5CB [6] is where a homeotropic sample is stabilized by **B** and destabilized by impressing an *ac* **E** field along the sample planes [7, 8]. Two different mathematical models [9, 10] have been proposed to explain the occurrence of *PD* in the above cases. It is necessary to establish whether the experimentally observed transitions are of a purely dielectric nature or involve conductivity. The electrical conductivities of a typical, impure nematic may change over the frequency range 0-1500 Hz [11].

EXPERIMENTAL SET UP AND METHOD OF OBSERVATIONS

The experimental set up and sample preparation are similar to those employed earlier (see figure 1 of reference [12]). Thick cells (see Table 1) are constructed using flat

sheet electrodes made of stainless steel.

TABLE 1 Dimensions of cells

Cell Number	Thickness (μm)	Electrode Gap (mm)	Reference
1	640	4.68	Fig. 1, 5
2	584	4.84	Fig. 2, 3
3	610	5.16	Fig. 3
4	200	3.80	Fig 4

The initial orientation $\mathbf{n}_0$ is along z which is also the direction of the stabilizing **B** field. The electrodes are in the yz plane so that initially, **E** is directed along x. *AC* voltage is measured in *rms* volts. The cell is housed in a thermostat which achieves long term temperature stability of better than ±10 mK around a mean temperature of 28° C. Thresholds for the onset of orientational instabilities are optically monitored using the video technique described before [12]. Photovoltage measurements are also performed with light from a He - Ne laser incident along z on the center of the sample. At a fixed **B** field, the voltage applied between the electrodes is ramped up from zero at a steady rate of 2.3 10^{-3} V/s. An initial rise in intensity of the photodiode trace in the presence of crossed polarizers with applied voltage indicates a clear trend of field induced pretransitional biaxiality [8].

Phase Diagrams for the Modulated Phase

Phase diagrams for different deformations are obtained in the *V–B* plane. Initially, a typical sequence of observations is described with emphasis on the high frequency regime. When voltage is increased from zero at a fixed **B** field, a cloudy region appears near one of the electrodes. On further increase of voltage, a similar cloud starts to form near the other electrode. The first cloudy region is monitored as voltage is continuously enhanced; then, modulations appear inside the cloud near the electrode. Depending upon the strength of **B** and the frequency, the modulations may be along y (*X* stripes; Figure 1a), along x (*Y* stripes; Figure 1c) or in the xy plane (*XY* stripes; Figure 1b). As soon as the stripes are resolved enough to be identified as periodic, the voltage across the cell is noted (say, V_{th}); this is taken to be the threshold for the onset of the given *PD*. The voltage can be increased further to find out how the modulated phase evolves in other regions of the sample. At a voltage slightly higher than V_{th}, stripes manifest in the second cloudy region near the other electrode. At a still higher voltage, the two banded regions travel towards the center of the cell where they merge to result in static *XY* stripes . The *XY* stripes appear to form as a consequence of 'curling up' of the

original *X* or *Y* stripe. When the voltage is ramped up further, the *XY* stripes grow fainter and start disappearing; finally, the cell becomes stripe-free. A polarization test shows **n** to be aligned along *x* axis. The above scenario is typical of strong stabilizing magnetic strengths, $B > 1000$ G.

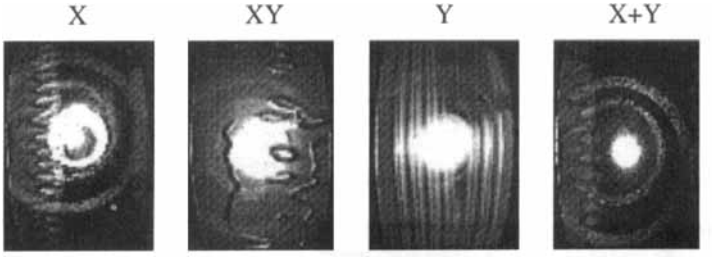

FIGURE 1a FIGURE 1b FIGURE 1c FIGURE 1d

Modulated Phase at 1500 Hz

Figure 2 below contains the phase diagram obtained with cell 1 at $f = 1500$ Hz.

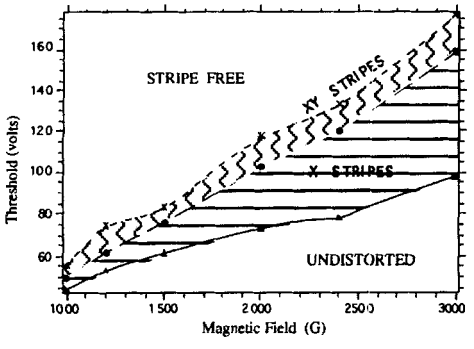

FIGURE 2 Phase Diagram at 1500 Hz

Frequency Dependence of Thresholds

The effect of frequency on the onset of instability is studied in the absence of **B**. The results of photovoltage measurement are presented in Figure 3. For a given cell, the threshold remains more or less constant in the higher frequency range but as frequency diminishes to around 200 Hz, the threshold also decreases. This reinforces the conclusion that the phenomenon on hand is definitely mediated by electrical conductivity. Two distinct reasons can be attributed for this. Firstly, the threshold for onset of instabilities becomes frequency dependent even when the individual conductivities are assumed to be frequency independent [13]. Secondly, the individual electrical conductivities of a nematic are themselves known to vary with the frequency of the applied field in some materials, especially in the low frequency range [11].

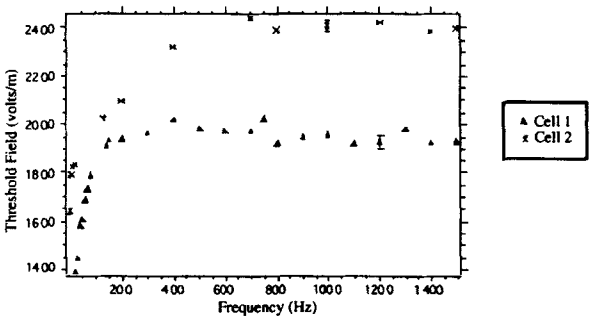

FIGURE 3 Electric threshold versus frequency at zero magnetic field

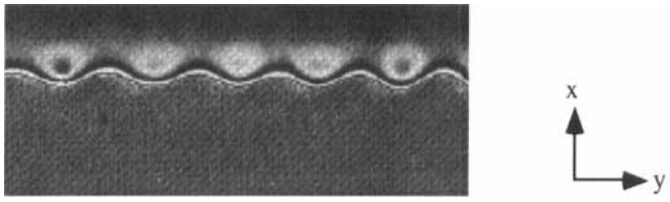

FIGURE 4 Modulation of the edge of cloudy region $f = 1500$ Hz; $B = 0$

Visual observations have been made for the $B = 0$ case at different frequencies. A fascinating variety of deformations and effects have been seen, many similar to those observed in [14]; details of these will be given elsewhere. At 1500 Hz when the applied voltage is ramped up, a cloud-like entity appears near one electrode; at a slightly higher voltage, a similar cloud appears near the other electrode also, indicating some asymmetry in the sample. As the voltage is increased, the cloudy regions start expanding into the body of the sample and at a certain voltage the edges of the cloudy regions appear modulated as shown in Figure 4. Eventually, the cloudy regions merge midway between the two electrodes forming a sharp line directed along y axis; the line is not straight but wavy. Schell and Porter [14] have reported similar observations in thin samples. They find that under decrease of voltage, the observations are reversible. In the present case, it is found that decrease of voltage leads to hysterisis (see Table 2).

TABLE 2 Hysterisis data ($B = 0$ is photovoltage data)

B (Gauss)	Deformation	Ramp up V_{th}	Ramp down V'_{th}	Hysterisis Width
0	HD	12.07	5.35	6.72
1500	X Stripe	57.10	55.39	1.71
1500	Stripe-free	84.57	78.94	5.63

To test if the stripe threshold is also a function of frequency in the presence of **B**, 1000 G was applied to the aligned sample. The voltage at each frequency is increased from zero and the stripe threshold and photodiode threshold are plotted in Figure 5 as functions of frequency. In general, the photodiode threshold is consistently higher than the visual threshold. The difference between the two thresholds shows that when a distortion appears near the electrodes, **n** near the sample center is relatively undeformed.

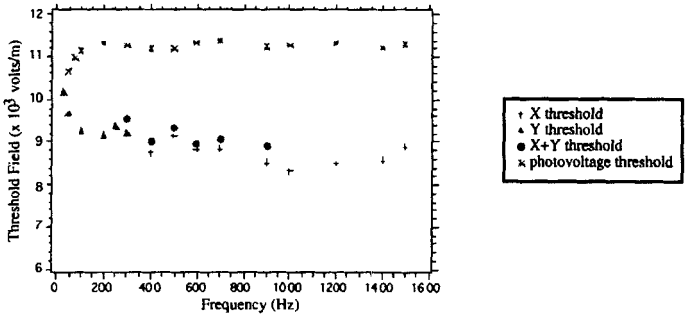

FIGURE 5 Variation of stripe threshold with frequency at $B = 1000$ G

(i) The high frequency range, $900 < f < 1500$ Hz. Only X stripes are observed at and slightly above threshold.

(ii) The middle frequency range, $300 < f < 900$ Hz. In this range, a new deformation appears above a well defined, second threshold when voltage is increased at a given frequency; we refer to this as the $X + Y$ stripes. The resulting deformation appears to have a mixture of the X and the Y stripes (Figure 1d).

(iii) The low frequency range, $30 < f < 300$ Hz. For $f < 300$ Hz, X stripes do not form at all. The deformation that appears at and slightly above threshold is Y stripe.

The frequency dependence of the thresholds (Figures 3, 5) is a strong indicator that the instability mechanism is not of only dielectric origin as considered previously [7, 8, 12]. To test for the presence of flow effects, a cell was constructed and filled with the nematic doped with a small quantity of fine chalk dust. A cellular flow was observed under a fixed **B** and $V > V_{th}$. At zero **B** field and a frequency of 5 Hz, a thinner cell with $V > V_{th}$ revealed fluctuating domains indicating turbulent flow with **n** changing continuously in a random way. In this state, the sample scatters light strongly.

CONCLUSIONS

Considering that in the present experiments, **n** near the electrodes gets deformed before *PD* sets in, the approach of [9] should become most suitable for deducing the *PD* threshold. Clearly, *PD* should initially develop near the electrodes where the modification of **E** is maximum. Manifestations of effects involving some sort of a cutoff frequency are found in the present work. The appearance of *PD* initially only near the electrodes as well as the build up of pretransitional (optical) biaxiality strongly indicate inhomogeneity in **E** occurring even before threshold is reached. The nature of *PD* shows marked dependence on frequency, especially when frequency is low. The *PD* threshold also varies strongly in this regime. This is proof of the involvement of electrical conductivity and its increasing involvement especially for low frequency and *dc* excitation. How a mathematical model can be built for the purpose of quantitative interpretation of these results is shown in Ref.[17].

REFERENCES

1. P.G. de Gennes and J.Prost, The Physics of Liquid Crystals (Clarendon Press, Oxford, 1993).
2. L.M. Blinov and V.G. Chigrinov, Electrooptic Effects in Liquid Crystal Materials (Springer-Verlag, New York, 1993).
3. R.B. Meyer, Phys. Rev. Lett. 22, 918 (1969).
4. H.J. Deuling, Solid State Phys. Suppl. 14, 77 (1978).
5. I. Dozov, G. Barbero, J.F. Palierne and G. Durand, Europhys. Lett. 1, 563 (1986).
6. P.G. Cummins, D.A. Dunmur and D.A. Laidler, Mol. Cryst. Liquid Cryst. 30, 109 (1975); J.D. Bunning, T.E. Faber and P.L. Sherrell, *J. de Physique* 42, 1175 (1981).
7. B.J. Frisken and P. Palffy-Muhoray, Phys. Rev. A 39, 1513 (1989).
8. B.J. Frisken and P. Palffy-Muhoray, Liq. Cryst. 5, 623 (1989).
9. D.W. Allender, B.J. Frisken and P. Palffy-Muhoray, Liq. Cryst. 5, 735 (1989).
10. U.D. Kini, J. de Physique (Paris) 51, 529 (1990).
11. M. Schadt and C. von Planta, J. Chem. Phys. 63, 4379 (1975).
12. S. Garg, S. Saeed and U.D. Kini, *Phys. Rev. E* 51, 5846 (1995).
13. Orsay Liquid Crystals Group, Mol. Cryst. Liquid Cryst. 12, 251 (1971);
14. K.T. Schell and R.S. Porter, *Mol. Cryst. Liquid Cryst.* 174, 141 (1989).
15. D.W. Allender, R.M. Hornreich and D.L. Johnson, Phys. Rev. Lett. 59, 2654 (1989).
16. E.F. Carr, Mol. Cryst. Liquid Cryst. 7, 253 (1969); W. Helfrich, J. Chem. Phys. 51, 4092 (1969).
17. S. Garg, S. Saeed, S. Wild, E. Bramley, and U.D. Kini, sub. to *Phys. Rev. E* (1996).

ACKNOWLEDGMENTS

Bramley and Wild acknowledge support provided by NSF-REU Grant DMR-9322301.